

## Tidal triggers and the predictability of solar activity

FRANK STEFANI,<sup>1</sup> GERRIT M. HORSTMANN,<sup>1</sup> GEORGE MAMATSASHVILI,<sup>1,2</sup> AND TOM WEIER<sup>1</sup>

<sup>1</sup>*Institute of Fluid Dynamics, Helmholtz-Zentrum Dresden-Rossendorf, Bautzner Landstrasse 400, 01328 Dresden, Germany*

<sup>2</sup>*Abastumani Astrophysical Observatory, Mount Kanobili, Abastumani 0301, Georgia*

### ABSTRACT

Magneto-Rossby waves in the solar tachocline are currently considered to be one of the main determinants of solar activity. In particular, they can give rise to the quasi-biennial oscillation (QBO). The latter was recently shown to be dominated by a phase-stable period of around 1.7 years. By analyzing 72 ground-level enhancement (GLE) events and 37 S-flares, we determine that this period is close to 1.723 years. This, in turn, is the dominant beat between the periods of the spring tides of the tidally dominant planets Venus, Earth, and Jupiter, which are suspected to synchronize not only the QBO, but also the 11.07-year Schwabe cycle. We demonstrate that recent events, such as the solar storm of 2024 May 10 and the strong X-flare of 2026 February 1, align well with maxima of the combined tidal forcing.

*Keywords:* Solar physics; Solar dynamo; Tidal Interaction

### 1. INTRODUCTION

The importance of Rossby waves for terrestrial weather systems and their predictability has been recognized for almost a century (Rossby 1939). However, Rossby waves may also play a key role in space weather which is governed by solar activity (Zaqarashvili et al. 2010a,b; Dikpati 2012; Márquez-Artavia et al. 2017; Dikpati et al. 2018; Zaqarashvili et al. 2021). As first discussed by Zaqarashvili et al. (2010b), they can naturally explain the Sun’s quasi-biennial oscillations (QBO).

Using the shallow-water magnetohydrodynamic approximation, these authors demonstrated that the interaction between differential rotation and a toroidal magnetic field exceeding  $10^5$  G leads to the instability of magneto-Rossby waves with a period of approximately two years. Later on, [Raphaldini & Raupp \(2015\)](#) argued that the dynamics of a resonant triad of magneto-Rossby waves could lead to periodically changing wave amplitudes with periods comparable to the dominant 11-year Schwabe cycle.

In addition to the huge energy reservoirs provided by differential rotation and toroidal magnetic fields, there are other sources that can cause neutrally stable Rossby waves to become unstable. One of them was recently discussed by [Horstmann et al. \(2023\)](#) who considered the tidal forces exerted by the revolving planets on the Sun. When forced by realistic-amplitude tides, magneto-Rossby waves were shown to acquire velocities of the order of m/s or larger, depending on a damping parameter whose precise value is, however, still unknown. Based on this result, it was demonstrated by [Stefani et al. \(2024\)](#) that the two-planet spring tides of Venus-Jupiter (with period 118 days), Earth-Jupiter (199 days), and Venus-Earth (292 days) lead to a beat period of 11.07 years which corresponds remarkably well to the Schwabe cycle. Saturn, whose tidal effect on the Sun is much weaker, only comes into play when considering the rosette-like barycentric motion of the Sun, which is known to be governed by the 19.86-year Jupiter-Saturn synodic cycle. While the internal flow structure triggered by the interaction of this barycentric motion with the Sun's rotation around its  $7^\circ$  inclined axis is still under scrutiny ([Shirley 2023](#); [Pierron & Forget 2026](#)), its inclusion in our dynamo model via a parametrization produced a long-term solar activity spectrum that remarkably aligns with that observed in climate-related sediments from Lake Lisan (see Figure 9 in [Stefani et al. \(2024\)](#)). The most striking feature of the emerging spectral peaks is the 193-year beat period, which appears to correspond to the Suess-de Vries cycle.

Yet another, much shorter beat period of 1.723 years was revealed by [Stefani et al. \(2025\)](#) and shown to coincide precisely with the dominant period underlying the occurrence of ground level enhancement (GLE) events. This work also confirmed the remarkable finding of [Velasco Herrera et al. \(2018\)](#) that those GLE events exhibit phase stability over nearly six solar cycles.

In view of this phase stability, and the time lag of approximately 1.7 years between the solar storm of 2024 May 10 and the strong X-class flare of 2026 February 1, it is tempting to take a closer look into the potential predictability of space weather events<sup>3</sup>. This is precisely the subject matter of the present paper. It goes beyond our previous work (Stefani et al. 2025) in two respects. Firstly, in addition to the 72 GLE events, we will analyze a series of 37 S-class events for which we will also find phase stability with a dominant period that is very close to that of the GLE events.

Secondly, we will compute the correlations of a merger of GLE and S-flare data not only with a single cosine function, but also with the actual beat signal resulting from the superposition of the three planetary tidal triggers. We will see that a significant portion of the events occur very close to the peaks of that beat signal. This particularly applies to the solar events of 2024 May 10 and 2026 February 1.

The paper will close with some conclusions and an outlook on further work.

## 2. GROUND LEVEL ENHANCEMENT EVENTS

In this section we revisit the GLE events that were analyzed previously by Velasco Herrera et al. (2018) and Stefani et al. (2025). These sporadic events are related to relativistic solar particles that produce air showers, the effects of which can be measured at ground level by a network of detectors. Table 1 and Figure 3 of Velasco Herrera et al. (2018) revealed that the 56 considered GLE events occurred preferentially in the positive phase of an oscillation with a period of 1.73 years which indeed points to a clocked process that was phase stable over approximately six solar cycles.

In Stefani et al. (2025) we had re-analyzed these GLE data, updating them from the 56 events used in Velasco Herrera et al. (2018) to the 71 events provided by the database of neutron monitor count rates at <https://gle.oulu.fi>. To precisely determine the best-fit period, we replaced the inverse

<sup>3</sup> When asked by spaceweather.com about the potential impact of the upcoming Venus-Earth-Jupiter alignment on solar activity, one of us (F.S.) made on 2026 January 7 the following prediction: “If the alignment excites magneto-Rossby waves as our model predicts, we might expect a higher probability of strong solar activity 40 to 60 days from now” (<https://spaceweather.com/archive.php?view=1&day=07&month=01&year=2026>). Unfortunately, due to a bug in the underlying code, this estimate was off by one month and should have read “10 to 30 days from now”, which would have included the 2026 February 1 event. Further details on that issue will be discussed below.

**Table 1.** Numbers, dates in the format YYYY/MM/DD, and days elapsed since 1955/12/31 of the 72 GLE events considered here. Note the beginning of the numbering with 5, and the missing event 17, according to the dataset provided at <https://gle.oulu.fi> .

No	Date	Days	No	Date	Days	No	Date	Days
5	1956/02/23	54	30	1977/11/22	7997	54	1992/11/02	13456
6	1956/08/30	243	31	1978/05/07	8163	55	1997/11/06	15286
7	1959/07/17	1294	32	1978/09/23	8302	56	1998/05/02	15463
8	1960/05/04	1586	33	1979/08/21	8634	57	1998/05/06	15467
9	1960/09/03	1708	34	1981/04/10	9232	58	1998/08/24	15577
10	1960/11/12	1778	35	1981/05/10	9262	59	2000/07/14	16267
11	1960/11/15	1781	36	1981/10/12	9417	60	2001/04/15	16542
12	1960/11/20	1786	37	1982/11/26	9827	61	2001/04/18	16545
13	1961/07/18	2026	38	1982/12/08	9839	62	2001/11/04	16745
14	1961/07/20	2028	39	1984/02/16	10274	63	2001/12/26	16797
15	1966/07/06	3840	40	1989/07/25	12260	64	2002/08/24	17038
16	1967/01/28	4046	41	1989/08/16	12282	65	2003/10/28	17468
18	1968/09/29	4656	42	1989/09/29	12326	66	2003/10/29	17469
19	1968/11/18	4706	43	1989/10/19	12346	67	2003/11/02	17473
20	1969/02/25	4805	44	1989/10/22	12349	68	2005/01/17	17915
21	1969/03/30	4838	45	1989/10/24	12351	69	2005/01/20	17918
22	1971/01/24	5503	46	1989/11/15	12373	70	2006/12/13	18610
23	1971/09/01	5723	47	1990/05/21	12560	71	2012/05/17	20592
24	1972/08/04	6061	48	1990/05/24	12563	72	2017/09/10	22534
25	1972/08/07	6064	49	1990/05/26	12565	73	2021/10/28	24043
26	1973/04/29	6329	50	1990/05/28	12567	74	2024/05/11	24969
27	1976/04/30	7426	51	1991/06/11	12946	75	2024/06/08	24997
28	1977/09/19	7933	52	1991/06/15	12950	76	2024/11/21	25163
29	1977/09/24	7938	53	1992/06/25	13326	77	2025/11/11	25518

wavelet method of Velasco Herrera et al. (2018) by computing the correlation coefficient

$$r = 1/N \sum_{i=1}^N \cos(2\pi t_i/T_0 + \varphi_0) \quad (1)$$

of  $N = 71$  GLE instants  $t_i$ , using cosine functions with variable periods  $T_0$  and phases  $\varphi_0$ . While  $r$  is not exactly Pearson's empirical correlation coefficient, it shares with it the main property of lying between -1 and 1. The latter value only occurs when the events and the cosine's maxima are perfectly aligned.

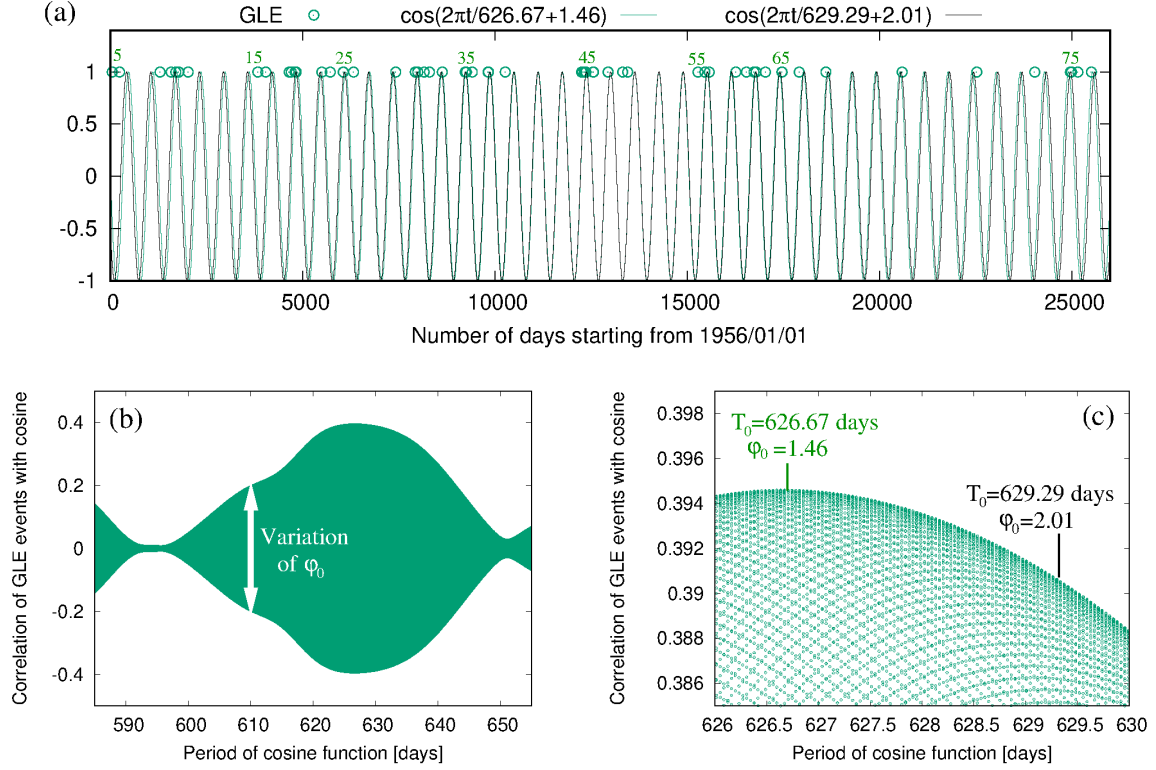


**Figure 1.** Analysis of GLE data. (a) Distribution of 72 events (green open circles) observed between 1956 February and 2025 November, as obtained from <https://gle oulu.fi>. The abscissa shows the time  $t$  in days starting from 1956 January 1. A few event numbers referring to Table 1 are indicated. The green curve shows the optimum cosine function  $\cos(2\pi t/626.67 + 1.46)$  that maximizes the correlation coefficient given in Equation (2). The black curve displays  $\cos(2\pi t/629.29 + 2.01)$  that results from the phase optimization when the theoretical period of  $T_0 = 629.29$  days is fixed beforehand. (b) Correlation coefficient of the 72 GLE events with cosine functions with variable periods  $T_0$  and phases  $\varphi_0$ . For each period  $T_0$ , the vertical extent emerges when varying  $\varphi_0$  between 0 and  $2\pi$ . (c) Zoomed-in version of (b), showing the maximum of Corr appearing for  $T_0 = 626.67$  days and  $\varphi_0 = 1.46$ . If the period is fixed beforehand to  $T_0 = 629.29$  days, we obtain a slightly decreased correlation coefficient for an optimum  $\varphi_0 = 2.01$ . These periods and phases are used for defining the green and black curves in (a).

Figure 8 of Stefani et al. (2025) showed a maximum correlation of 0.2964 for a period of 629.85 days, which corresponds to 1.724 years. This value is indeed remarkably close to the value of 1.723 years we had derived as the dominant beat of the tidally triggered magneto-Rossby waves.

In the following, two modifications will be applied. Firstly, we correct a timing error in Stefani et al. (2025) that led to an incorrect phase of  $\varphi_0 = 1.88$ , when it should have been  $\varphi_0 = 2.19$ . While

this phase error (equivalent to a time shift of 31 days) had no effect on the main message of [Stefani et al. \(2025\)](#), it will be important later on when considering the predictability of the solar events of early 2026.

Secondly, from here on we will use a modified measure of correlation in the form

$$\text{Corr} = \frac{\sum_{i=1}^N \cos(2\pi t_i/T_0 + \varphi_0)}{\sqrt{\sum_{i=1}^N \cos^2(2\pi t_i/T_0 + \varphi_0)}} \quad (2)$$

which is closer in spirit to Pearson's correlation coefficient between events (characterized by a number 1) and the underlying cosine function. We select this metric having in mind its straightforward transferability to more complex functions. Yet, in Appendix A, we will revisit the correlation  $r$ , as defined in Equation (1), when employing the Rayleigh test, which is the standard method for detecting periodicity in unevenly distributed data ([Dröge et al. 1990](#)).

Table 1 lists the 72 GLE events between February 1956 and November 2025. The results of the data analysis are shown in Figure 1. Panel (a) displays the distribution of the 72 GLE events over time. Panels (b) and (c) illustrate the determination of the optimal period  $T_0 = 626.67$  days and phase angle  $\varphi_0 = 1.46$ , which are used to define the green curve in panel (a). Additionally, we also determine the optimum phase when fixing  $T_0$  beforehand to the theoretical value of 629.29 days as derived from the Rossby-wave theory. The resulting cosine function is displayed in black in panel (a). The two curves are almost indistinguishable from each other, with a mere 0.4 per cent difference in period. This suggests that the underlying theory may indeed have some merit. Note also that the two correlation values obtained, 0.394 and 0.391, correspond to two-sided  $p$ -values of 0.00062 and 0.00068 for a sample size of 72, which indicates a high level of significance for the correlation. Admittedly, since Corr is not exactly a Pearson correlation coefficient, those  $p$ -values should be interpreted with some caution.

### 3. S-CLASS FLARES

In this section we apply the methodology outlined in the previous section to the 37 events of solar superflares of S-class ( $>X10$  in soft X-rays) that were recorded since 1978 ([Tan et al. 2025](#)). The occurrence of these S-flares was recently shown in the wavelet analysis of [Velasco Herrera et al. \(2026\)](#)

**Table 2.** Number, dates in the format YYYY/MM/DD, and days elapsed since 1955/12/31 of the 37 S-flare events considered here. The data are from [Tan et al. \(2025\)](#) and [Velasco Herrera et al. \(2026\)](#).

No	Date	Days	No	Date	Days	No	Date	Days
1	1978/7/11	8228	14	1990/5/24	12563	27	2001/4/15	16542
2	1980/11/6	9077	15	1991/1/25	12809	28	2003/10/28	17468
3	1982/6/3	9651	16	1991/3/4	12847	29	2003/10/29	17469
4	1982/6/6	9654	17	1991/3/22	12865	30	2003/11/2	17473
5	1982/7/12	9690	18	1991/6/1	12936	31	2003/11/4	17475
6	1982/12/15	9846	19	1991/6/4	12939	32	2005/1/20	17918
7	1982/12/17	9848	20	1991/6/6	12941	33	2005/9/7	18148
8	1984/4/24	10342	21	1991/6/9	12944	34	2006/12/5	18602
9	1984/5/20	10368	22	1991/6/11	12946	35	2011/8/9	20310
10	1989/3/6	12119	23	1991/6/15	12950	36	2017/9/6	22530
11	1989/8/16	12282	24	1992/11/2	13456	37	2017/9/10	22534
12	1989/9/29	12326	25	1997/11/6	15286	-	-	-
13	1989/10/19	12346	26	2001/4/2	16529	-	-	-

to be governed by coupled phase states of 1.7-year and 7-year oscillations. The dates of these events, taken from [Tan et al. \(2025\)](#) and [Velasco Herrera et al. \(2026\)](#), are listed in Table 2.

The data analysis is illustrated in Figure 2. Panel (a) shows the distribution of the 37 S-flare events, while in panels (b) and (c) the optimal periods  $T_0$  and phase angles  $\varphi_0$  are determined. Here, the best-fit period,  $T_0 = 637.92$  days, is a bit farther away (1.4 per cent) from the theoretical value of 629.29 days. For  $N = 37$ , the two correlations of 0.72 for the optimum period of 1.747 years and 0.64 for the theoretical period of 1.723 years have p-values as low as  $5.5 \times 10^{-7}$  and  $3.6 \times 10^{-5}$ , respectively, which implies an even higher significance of the correlations than in the GLE case.

#### 4. GLE AND S-FLARE EVENTS TAKEN TOGETHER

Given the very close results obtained for the best-fit periods of the 72 GLE events and the 37 S-flares, we decided to assess also a combined dataset of 109 events in total. This is illustrated in Figure 3. Here, the resulting best-fit period,  $T_0 = 632.88$  days, is only 0.6 per cent away from the theoretical value of 629.29 days. For  $N = 109$ , the two correlations of 0.435 for the optimum period of 1.733 years and 0.424 for the theoretical period of 1.723 years have p-values of  $3.2 \times 10^{-6}$  and  $6.7 \times 10^{-6}$ , respectively.

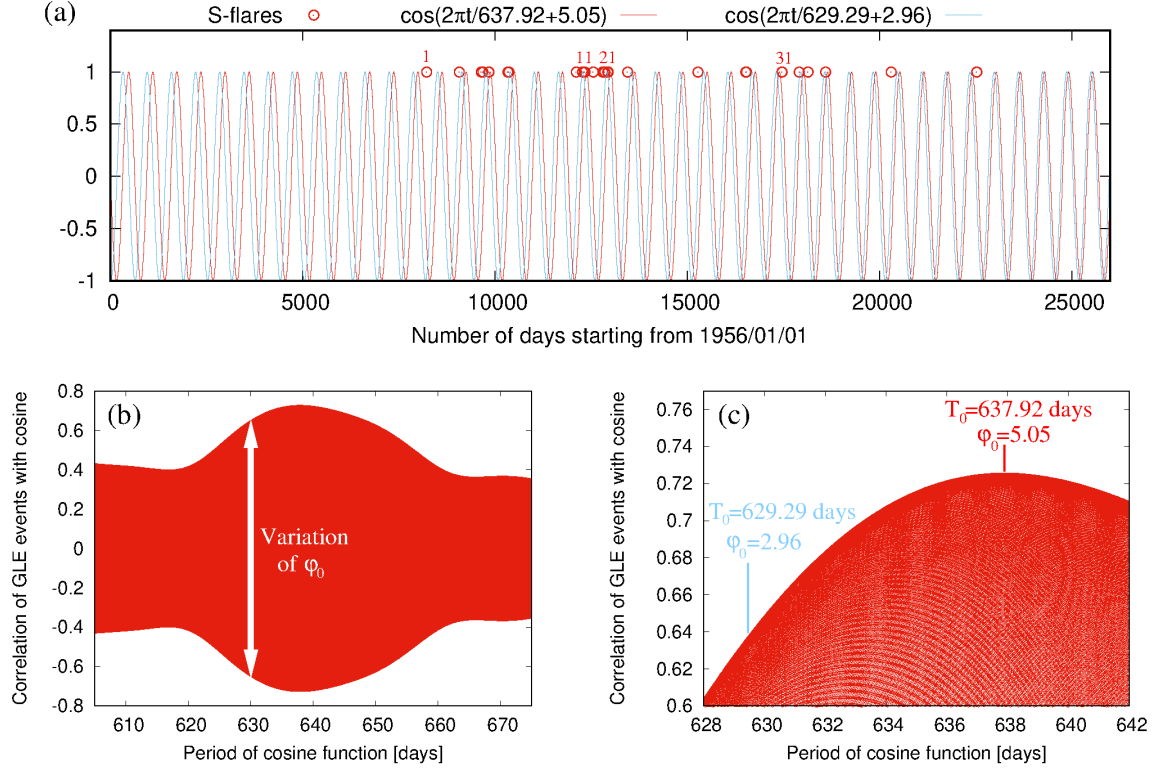


**Figure 2.** Same as Figure 1, but for the 37 S-flare events since 1978. Here, the red curve shows the optimum cosine function  $\cos(2\pi t/637.92 + 5.05)$  that maximizes Corr given in Equation (2). The light blue curve shows  $\cos(2\pi t/629.29 + 2.96)$  that results from the optimization of the phase when the theoretical period of  $T_0 = 629.29$  days is fixed beforehand.

While all previous analyses used simple cosines as test functions, in the following we move closer to the Rossby-wave mechanism underlying the synchronization theory of the solar dynamo that we have developed over the last decade (Weber et al. 2015; Stefani et al. 2016, 2019, 2021; Klevs et al. 2023; Horstmann et al. 2023; Stefani et al. 2024, 2025), building on previous work of Abreu et al. (2012); Scafetta (2012); Wilson (2013); Okhlopkov (2016).

Following Stefani et al. (2025), we first consider the sum of three equally weighted tidal wave excitations with periods of (approximately) 118 days, 199 days and 292 days that correspond to the two-planet spring-tides of Venus-Jupiter, Earth-Jupiter and Venus-Earth, respectively:

$$s(t) = \cos\left(2\pi \cdot \frac{t - t_{VJ}}{0.5 \cdot P_{VJ}}\right) + \cos\left(2\pi \cdot \frac{t - t_{EJ}}{0.5 \cdot P_{EJ}}\right) + \cos\left(2\pi \cdot \frac{t - t_{VE}}{0.5 \cdot P_{VE}}\right). \quad (3)$$

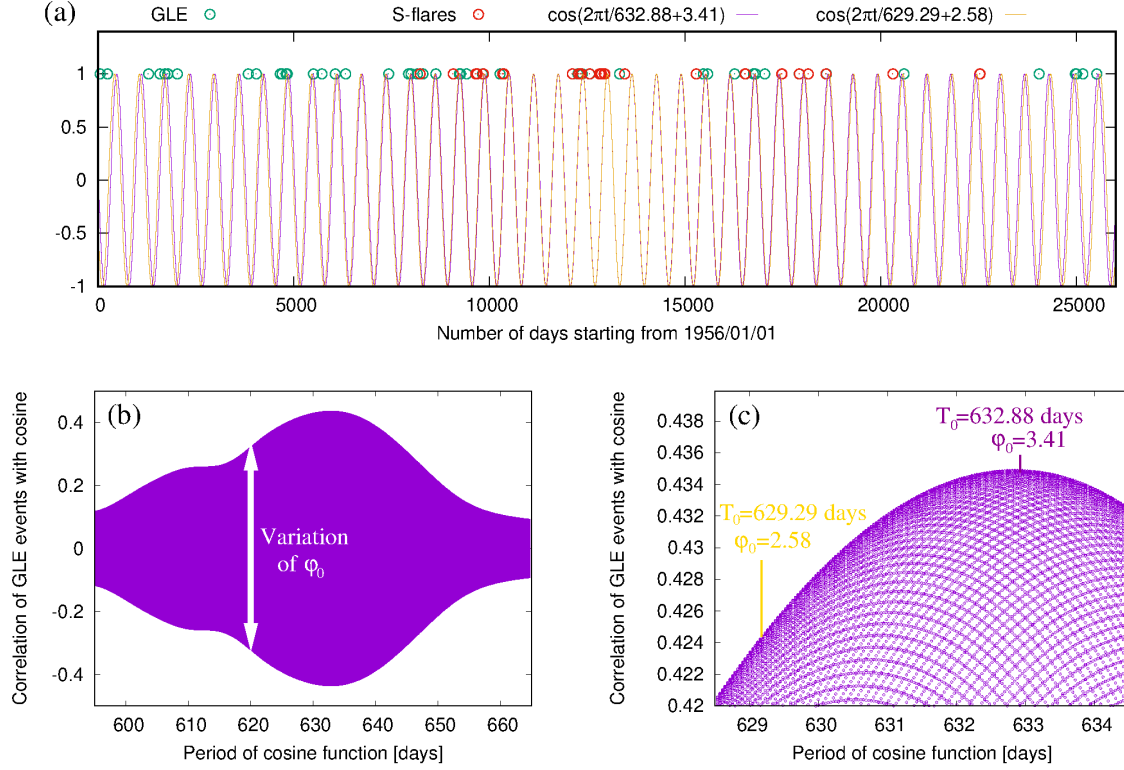


**Figure 3.** Same as Figure 1, but for the merger of the 72 GLE (green open circles) with the 37 S-flare events (red open circles). Here, the violet curve shows the optimum cosine function  $\cos(2\pi t/632.88 + 3.41)$ . The gold curve shows  $\cos(2\pi t/629.29 + 2.58)$  that results from the optimization of the phase when the theoretical period of  $T_0 = 629.29$  days is fixed beforehand.

To be more specific, we use the accurate two-planet synodic periods  $P_{VJ} = 0.64884$  years,  $P_{EJ} = 1.09207$  years,  $P_{VE} = 1.59876$  years, and the epochs of the corresponding conjunctions  $t_{VJ} = 2002.34$ ,  $t_{EJ} = 2003.09$ , and  $t_{VE} = 2002.83$  that were adopted from [Scafetta & Bianchini \(2022\)](#).

As shown by [Dikpati & McIntosh \(2020\)](#), magneto-Rossby waves lead to tachocline bulges and depressions in the top surface and can therefore play a role in providing longitude and latitude locations for emergence of toroidal fields into the convection zone and photosphere. Moreover, the maximum field-strength of toroidal flux tubes that can be stored in mechanical equilibrium at the bottom of the convection zone is very sensitive to the value of the superadiabaticity ([Abreu et al. 2012](#)). In this sense, the sum  $s(t)$  of the three tidal forcings might already be relevant for the excitation of tachocline deformations and the launching of flux tubes. However, in the following we will consider its square,  $s^2(t)$ , which may be more relevant for tachocline nonlinear oscillations

(TNO), modifications of zonal or meridional flows, or the wave-related helicity and the dynamo-relevant  $\alpha$ -effect.

The square  $s^2(t)$  of the sum of the three cosine functions is shown as the dark blue curve in panels (a) and (b) of Figure 4, together with the 72 GLE and 37 S-flare events. Compared to Figures 1, 2, 3, we have doubled the time-resolution in order to better recognize the frequent (although not perfect) coincidences of solar events with the spikes of  $s^2(t)$ . While the average distance between these spikes corresponds to the above-mentioned beat period of 1.723 years (629.29 days), they show a systematic oscillation leading to the additional 11.07-year beat period which can be recognized in the changing height of the spikes. As an aside, this second period is at the root of our parametric resonance model to describe the Schwabe cycle (Stefani et al. 2019; Klevs et al. 2023; Stefani et al. 2024, 2025).

In the following we will assess the correlation of the tidal forcing  $s^2(t)$  with the solar events which we define, in analogy to Equation (2), as

$$\text{Corr} = \frac{\sum_{i=1}^N [s^2(t_i) - \overline{s^2(t)}]}{\sqrt{\sum_{i=1}^N [s^2(t_i) - \overline{s^2(t)}]^2}} . \quad (4)$$

In this context, it seems also indicated to “smear out” the very spiky shape of  $s^2(t)$  by applying to it a moving average. Indeed, the toroidal magnetic field, on which the amplitudes of the three tidally excited magneto-Rossby waves depend, exhibits a complicated butterfly-type variation in space and time. While finding the most appropriate averaging procedure over space and/or time is non-trivial, we consider averaging over a small fraction of the Schwabe cycle to be reasonable. Three of those representative averages (with time-windows of 101, 201, and 301 days) are displayed in panels (a) and (b) of Figure 4 with different colors. For the original  $s^2(t)$  and the three time-averages we ask now which time-shift (backward or forward) would give the highest correlation with the solar event data. While formally this corresponds to the phase optimization for the single cosine functions as carried out in Figures 1, 2, and 3, now the time-shift has a clear physical meaning in that it describes the lag between the maximum tidal triggering of Rossby waves and the solar event that ultimately occurs at the solar surface. In view of the typical rise times of flux tubes in the order of a month or more (Weber et al. 2011), one would expect a similar time lag to come out as a sort of optimum.

However, the picture arising from panels (c) and (d) of Figure 4 is less clear. While in general the correlation peaks around zero time lag, in particular the dark blue curve of  $s^2(t)$  has a somewhat counterintuitive peak at a *positive* time shift of approximately 70 days with respect to the solar events. For longer time averages (yellow and gold), the correlation curves become much smoother and indeed peak around a zero time lag.

What is remarkable in this respect is the case of an average window of 101 days. For this window length the main peaks in panels (a) and (b) come to lie in between the peaks of the original signal  $s^2(t)$ .

In Appendix B, we will assess whether the correlation can still be improved by varying the pre-factors of the three individual waves, which entered Equation (3) with equal weights.

## 5. X-FLARE OF 2026 FEBRUARY 1

The high solar activities of early 2026 occurred approximately 1.7 years after the two GLE events of 2024 May and June. In this section, we will assess the possible connection between these events and the strong tidal forcings resulting from the alignment of Venus, Earth and Jupiter.

To start with, we display in Figure 5(a) the X8.3-class flare of 2026 February 1 (red full triangle) in the context of the solar events since late 1977 November (8000 days after 1955/12/31). We also plot  $s^2(t)$ , alongside the black, light blue and gold cosine curves from Figures 1, 2 and 3, which had come out as the best fits when the period was fixed beforehand to 629.29 days. Obviously, all these curves are very close to each other, and the spiky  $s^2(t)$  curve fits nicely into the picture, despite its slight wiggling to the left and right associated with the occurrence of double peaks. Overall, we also observe a significant, albeit not perfect, synchronism between the peaks of the four curves and the solar events.

The focus in panel (b) of Figure 5 is now on the last two years. On the left-hand side, we recognize the two GLE events that occurred on 2024 May 11 and 2024 June 8. Remarkably, the peak of  $s^2(t)$  lies almost exactly between these two closely neighboring events. Here, the idea that solar events are not related to the very maximum of the  $s^2(t)$  function, but to the neighbouring points of its steepest ascent or descent, comes to mind. Very close to  $s^2(t)$  lies the much wider black curve, representing

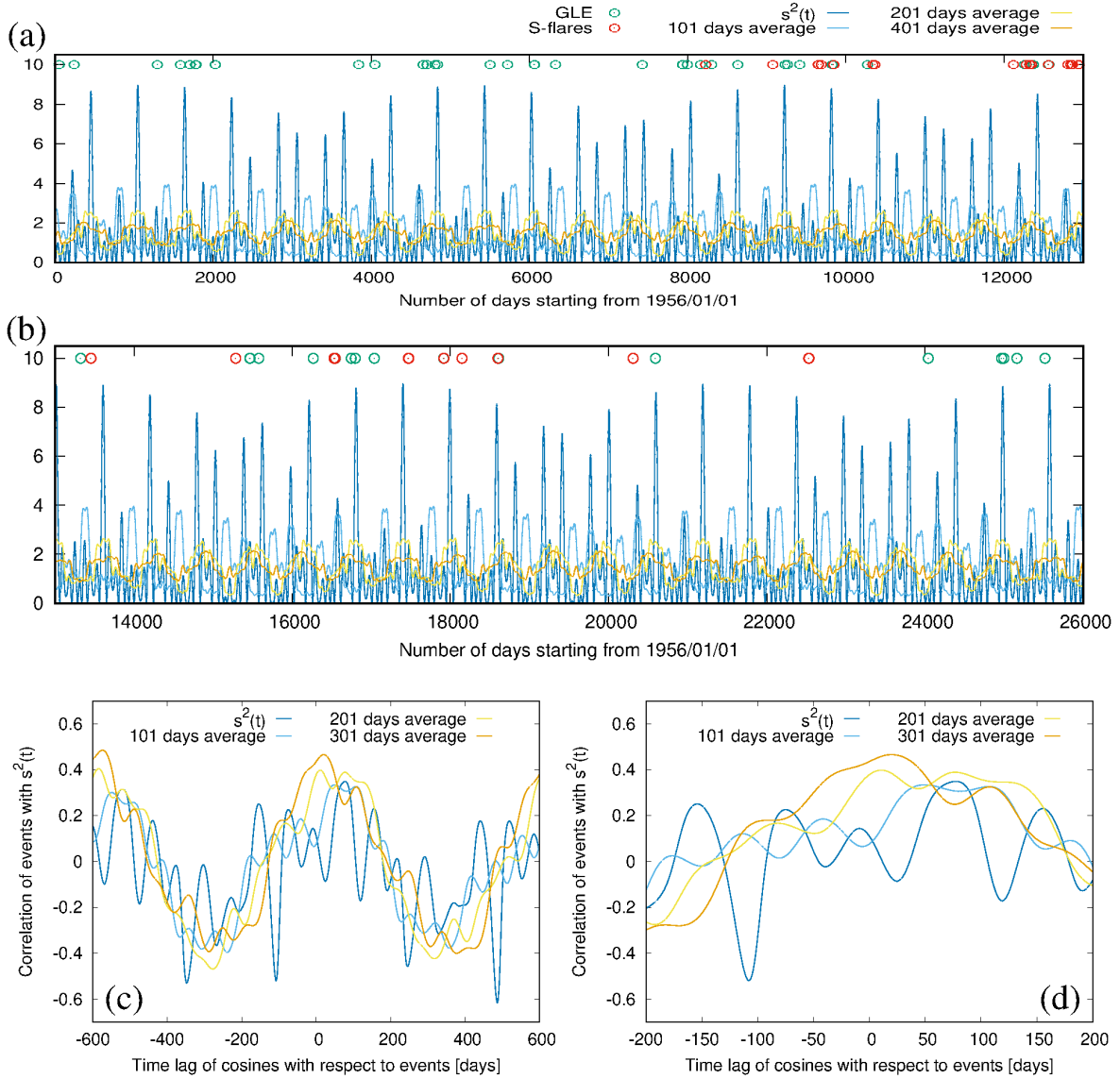


**Figure 4.** GLE and S-flare events,  $s^2(t)$ , and different time averages of it (a,b). The longer beat period of 11.07 years (corresponding to the Schwabe cycle) can be recognized in the varying height of the spikes. Correlation coefficients of the four curves from (a,b) with the solar events in dependence on the time-lag (c). The same, but zoomed in on shorter time lags (d).

the best-fit cosine function of the GLE events for the fixed 629.29-day period. The other two cosine curves (the light blue and gold ones) are shifted slightly towards earlier times. Turning to the right-hand side of panel (b), we see that the strong X-flare event of 2026 February 1 occurred only 23 days after the peak of  $s^2(t)$  located on 2026 January 9. While this corresponds nicely to the point

of steepest *descent* of  $s^2(t)$ , the preceding GLE event of 2025 October 25 occurred a bit too early to coincide with the point of steepest *ascent*.

The dates of the maxima of the pure cosines are also displayed in panel (b). Note that the sequence of the maxima of the dark blue and the black curve has interchanged between 2024 and 2026. While both have the same dominant period of 629.29 days,  $s^2(t)$  has slightly wiggled to the left.

In panel (c) we show the corresponding green, red and violet single-cosine curves from Figures 1, 2, 3 which were obtained when optimizing both the phases *and* the periods. Once again, we see a fairly good correlation with the solar events.

We note in passing that omitting the one GLE-event from 2025 in the determination of the optimal parameters leads only to a minor shift of the corresponding curves in Figure 5 by 3-16 days to the right.

In this context, let us finally take a look at the dashed and dotted green curves in panel (c). The dotted one,  $\cos(2\pi t/629.85 + 1.88)$ , was presented in [Stefani et al. \(2025\)](#) as the best fit when using the simplified correlation expression  $r = 1/71 \sum_{i=1}^{71} \cos(2\pi t_i/T_0 + \phi_0)$ . However, this solution was flawed due to a bug in the code, and it should have been the dashed green curve, i.e.  $\cos(2\pi t/629.77 + 2.19)$ . The 31-day difference between them explains the inaccuracy of the forecast made on 7 January 2026, as mentioned above. In any case, in view of the results obtained in the present paper, we would generally argue in favour of using  $s^2(t)$  instead of the cosine functions for any forecasting purposes. Indeed, both the two GLE events of 2024 and the strong X-flare of 2026 February 1 occurred very close to the peaks of  $s^2(t)$ . The timing of the latter event aligns closely with the expected one-month lag for the flux tubes to emerge on the Sun's surface ([Weber et al. 2011](#)), although this may be a coincidental occurrence. As mentioned above, it could also be the points of steepest ascent or descent that are decisive.

## 6. CONCLUSIONS

In this paper we have refined and deepened our previous examination of a potential link between extreme solar events and tidal triggers of magneto-Rossby waves at the solar tachocline. As for the GLE events, we found a correlation coefficient of 0.394 when using a cosine function with an

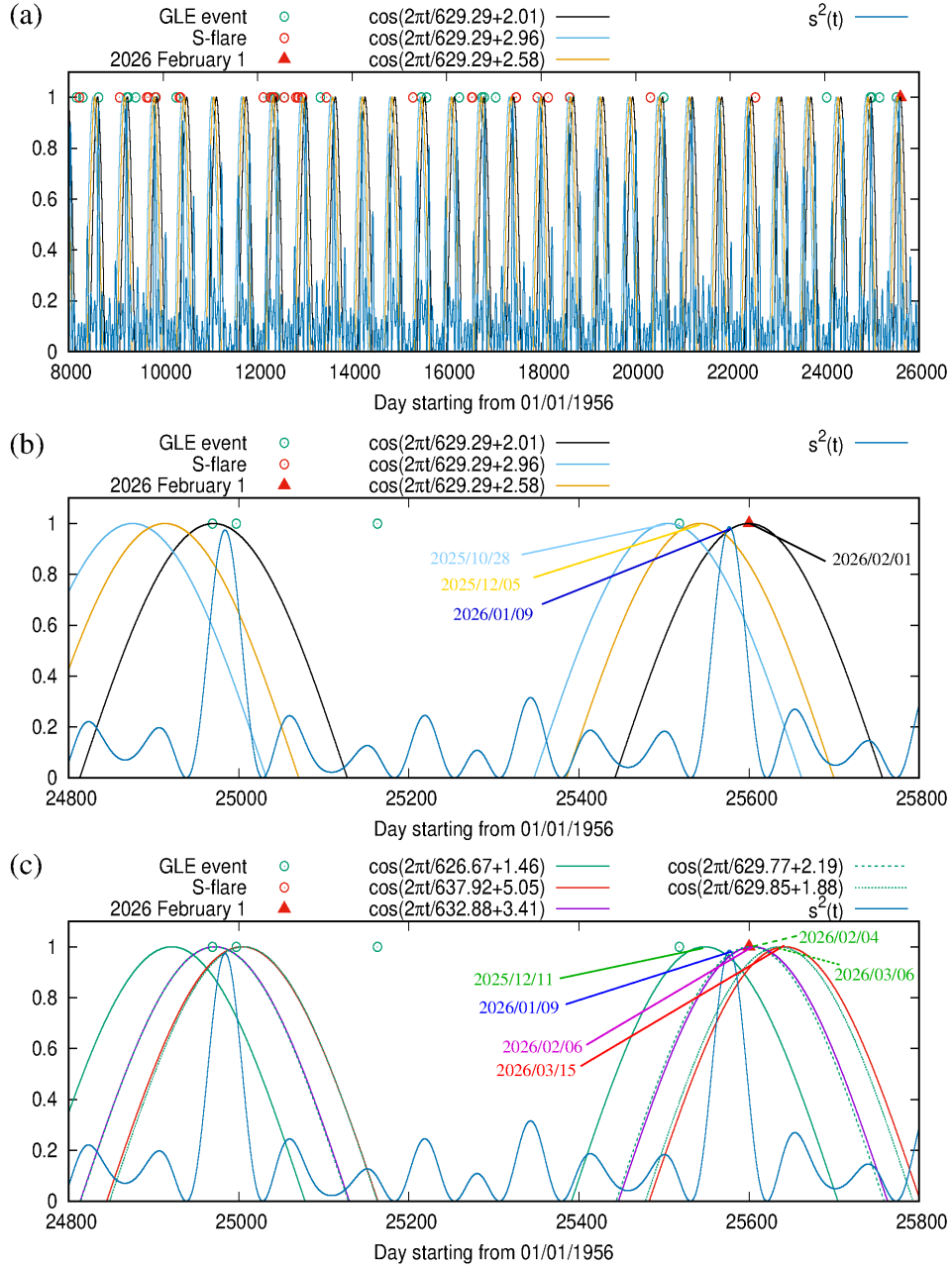


**Figure 5.** The 2026 February 1 event and its potential predictability. (a) GLE and S-flare events since 1977 November together with  $s^2(t)$  and the three optimized 629.29-day periodic functions. The strong X-flare of 2026 February 1 is added as a red triangle. (b) Details of (a) with the dates of the maxima of the four curves indicated. (c) Modification of (b) showing the curves with optimized phases  $\varphi_0$  and periods  $T_0$ . The dashed green curve with  $\varphi_0 = 2.19$  would result when using the correlation function without denominator. The dotted green line, with the erroneous phase  $\varphi_0 = 1.88$ , was given in Stefani et al. (2025). The phase difference corresponds to the time shift of 31 day by which the prediction for the early 2026 events was off.

optimized period of 1.716 years. Utilizing the theoretical beat period of 1.723 years gave a slightly reduced correlation of 0.391. For the 72 GLE events used, the corresponding low  $p$ -values pointed to a high significance of the correlations.

When applying the same method to the sequence of 37 S-class flares, we found even higher correlations of 0.72 and 0.64 for the optimized and theoretical periods of 1.747 and 1.723 years, respectively. The corresponding  $p$ -values were very low.

We also applied the method to a simple merger of the GLE and S-flare events. For the arising 109 events we obtained correlations of 0.434 for an optimum period of 1.733 years and 0.424 for 1.723 years, leading again to rather low  $p$ -values of  $3.2 \times 10^{-6}$  and  $6.7 \times 10^{-6}$ , respectively.

As shown in Appendix A, the use of the Rayleigh test instead of the correlation coefficient  $\text{Corr}$  leads only to minor modifications of our results.

Optimizing the functions with fixed periods for different sets of solar events results in a maximum phase difference of 15 per cent, equivalent to 95 days. This, along with the highly significant correlations, indicates a phase-stable process that governs the solar QBO.

For the merged data set, we also computed the correlation of the events with the square of the sum of the three tidal trigger functions which is dominated by steep peaks separated, on average, by gaps of 629.29 days (1.723 years). When shifting this function (and its various moving averages) backwards or forwards in relation to the solar events, we found that the maximum correlation typically occurred with a positive time lag of around 70 days. At first glance, this is surprising, since one would expect the reverse, meaning that tidal peaks should precede solar events. One possible explanation is the significant width (of approximately 100 days) of the main peaks of the  $s^2(t)$  curve, which could lead to flux tube launches already at the rising flank of the tidal trigger of the Rossby waves.

All this shows that we still have a long way to go before we understand the physical mechanism that links the excitation of magneto-Rossby waves by tides with the launching of flux tubes. It goes without saying that any viable forecast must also take into account the actual phase of the 11-year Schwabe cycle. In this context, the third harmonic of the Hale cycle may also play a role, as suggested by recent results of [Velasco Herrera et al. \(2026\)](#) and confirmed in Appendix A. Apart from this, we

must also acknowledge that although magneto-Rossby waves provide an ideal resonance ground for tidal forces to act upon, it cannot be ruled out that other mechanisms are at play.

In the future, we will assess how much further the correlations can be improved by taking into account the dependence of the weights of the three waves on the instantaneous toroidal field. It may also be worthwhile including somewhat less extreme events, such as X-flares and sub-GLE events, in the data analysis.

## APPENDIX A

In Sections 2-4 we have considered the correlation coefficient  $\text{Corr}$ , defined in Equation (2), as an appropriate metric that can be easily generalized to other test functions. In this Appendix, we apply the Rayleigh test to the datasets as a complementary method of establishing a connection with more standard techniques for determining dominant periods from non-evenly distributed data.

According to [Dröge et al. \(1990\)](#), the test statistic  $z$  used in the Rayleigh test is defined by

$$z(T_0) = \frac{1}{N} \left[ \left( \sum_{i=1}^N \cos(2\pi t_i/T_0) \right)^2 + \left( \sum_{i=1}^N \sin(2\pi t_i/T_0) \right)^2 \right]. \quad (5)$$

Again,  $t_i$  stands for the instants of the  $N$  extreme solar events under consideration, and  $T_0$  is the variable period. Note that the term in the square brackets corresponds to the square of the measure  $r$ , defined previously in Equation (1), when using therein the optimized phase  $\varphi_0$  that maximizes the sum of the cosine-terms, while zeroing the sum of the sine-terms. This lends plausibility to the notion  $z = Nr^2$  which is frequently used in the context of the Rayleigh test.

Figure 6 shows the  $z$ -values obtained when using the 72 GLE events (a,c), the 37 S-flare events (b,d), and the 109 merged events (e,f). Panels (a,c,e) on the left-hand side show the general picture of  $z(T_0)$  between 100 and 5000 days. In addition to the obvious QBO-peaks at  $T_Q$  around 629 days, we consistently observe a peak at approximately the 11-year Schwabe cycle period, which we denote by  $T_S$ . Due to the limited length of the data sets, this peak is very broad, so the indicated maxima should be interpreted with caution. Another clear peak appears approximately at two-thirds of the Schwabe period, denoted by  $T_{2/3S}$ . This triple harmonic of the Hale cycle, which played also a big role in [Velasco Herrera et al. \(2026\)](#), appears to be a fairly universal feature of oscillatory dynamos.

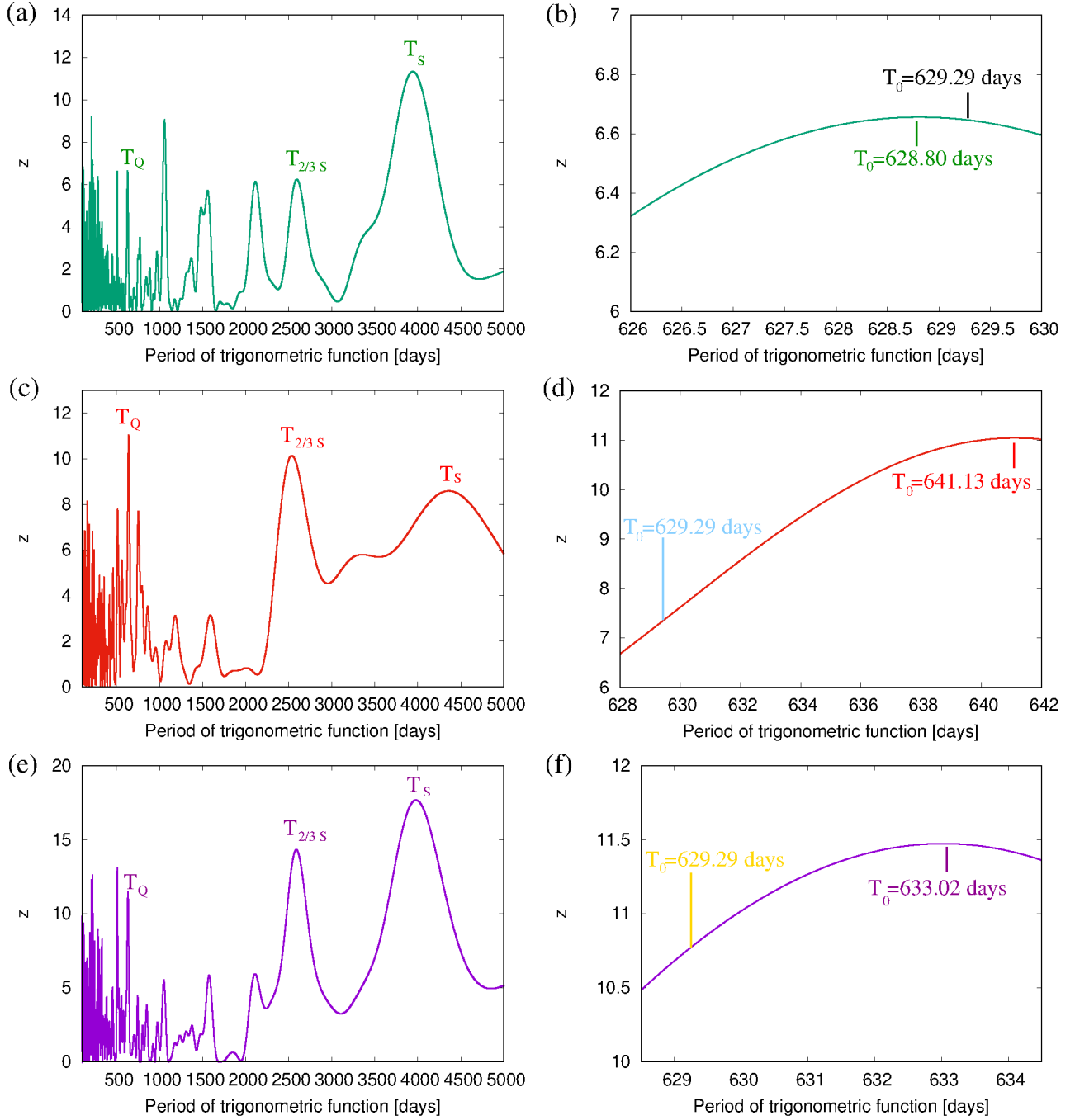


**Figure 6.** Results of the Rayleigh tests for the 72 GLE events (a,b), the 37 S-flare events (c,d), and the 109 merged events (e,f). The left column (a,c,e) shows the  $z$ -values between 100 and 5000 days, the right column shows the  $z$ -values in the vicinity of 629.29 days. Here, the chosen segment of the abscissa corresponds to those of the (c)-panels in Figures 1, 2 and 3. The specific  $z$ -values at the optimized  $T_0$  are, respectively, 6.66 (a), 11.04 (b), and 11.47 (c). The corresponding values at the theoretical QBO-period are, respectively, 6.65 (a), 7.27 (b), and 10.78 (c).

For example, it has also been observed in the Riga dynamo experiment (see, e.g., Figure 15 in [Gailitis et al. \(2018\)](#)). Note also that the peaks in the vicinity of  $T_0$  emerge as side peaks of its interaction with  $T_{2/3S}$ .

Now focusing on the very peaks at  $T_Q$ , we have chosen the segments of the abscissa on the right-hand side panels (b, d and f) to be equal to those of the respective (c)-panels of Figures 1, 2 and 3. When we compare those panels, we can see that the Rayleigh test yields slight shifts in the maxima. This is not surprising, given that the standard deviation of the values of the cosine-function in the denominator of Equation (2) is not included in Equations (1) and (4).

Apart from that subtlety, all peaks remain quite close to the theoretical QBO-period of 629.29 days. To derive the  $p$ -value for the Rayleigh power  $z$ , and the  $N$  events, we use the refined expression

$$p \approx e^{-z} \left[ 1 + \frac{2z - z^2}{4N} - \frac{24z - 132z^2 + 76z^3 - 9z^4}{288N^2} \right]. \quad (6)$$

For the 109 merged GLE and S-flare events, we obtain for  $z = 11.47$  (measured at the optimum  $T_0 = 633.02$  days) a  $p$ -value of  $8.0 \times 10^{-6}$ , and  $p = 1.6 \times 10^{-5}$  for the  $z = 10.78$  as measured at the theoretical QBO-period of 629.29 days. While both values are approximately 2.5 times larger than those obtained in Section 4 when using Corr, they are still very small, providing again strong evidence against randomness. Thus, the Rayleigh test strengthened the results obtained when using Equation (2) in the main analysis.

## APPENDIX B

In this Appendix, we take a closer look at the sum of the three waves in Equation (3) and consider the possibility that they may have different weights. In fact, Figures 2-4 of [Stefani et al. \(2024\)](#) indicate that both the absolute strengths and the relative weights of the three tidally-triggered magneto-Rossby waves depend on the instantaneous value of the toroidal field. Let us generalize Equation (3) to

$$s(t) = A \cos \left( 2\pi \cdot \frac{t - t_{VJ}}{0.5 \cdot P_{VJ}} \right) + B \cos \left( 2\pi \cdot \frac{t - t_{EJ}}{0.5 \cdot P_{EJ}} \right) + \cos \left( 2\pi \cdot \frac{t - t_{VE}}{0.5 \cdot P_{VE}} \right), \quad (7)$$

where A and B measure the relative weights of the first and second magneto-Rossby waves with respect to the third one. While for weak toroidal fields, Figure 2 of [Stefani et al. \(2024\)](#) would suggest

a rather low value of  $A$ , the breakdown of the excitation of the wave with  $P_{VE}$  at the strongest fields (see Figure 4 of that paper) would point to a large value of  $A$ . Since correctly incorporating this subtle dependence into our scheme requires much more effort, here we can only explore some generic consequences of changing the relative weights.

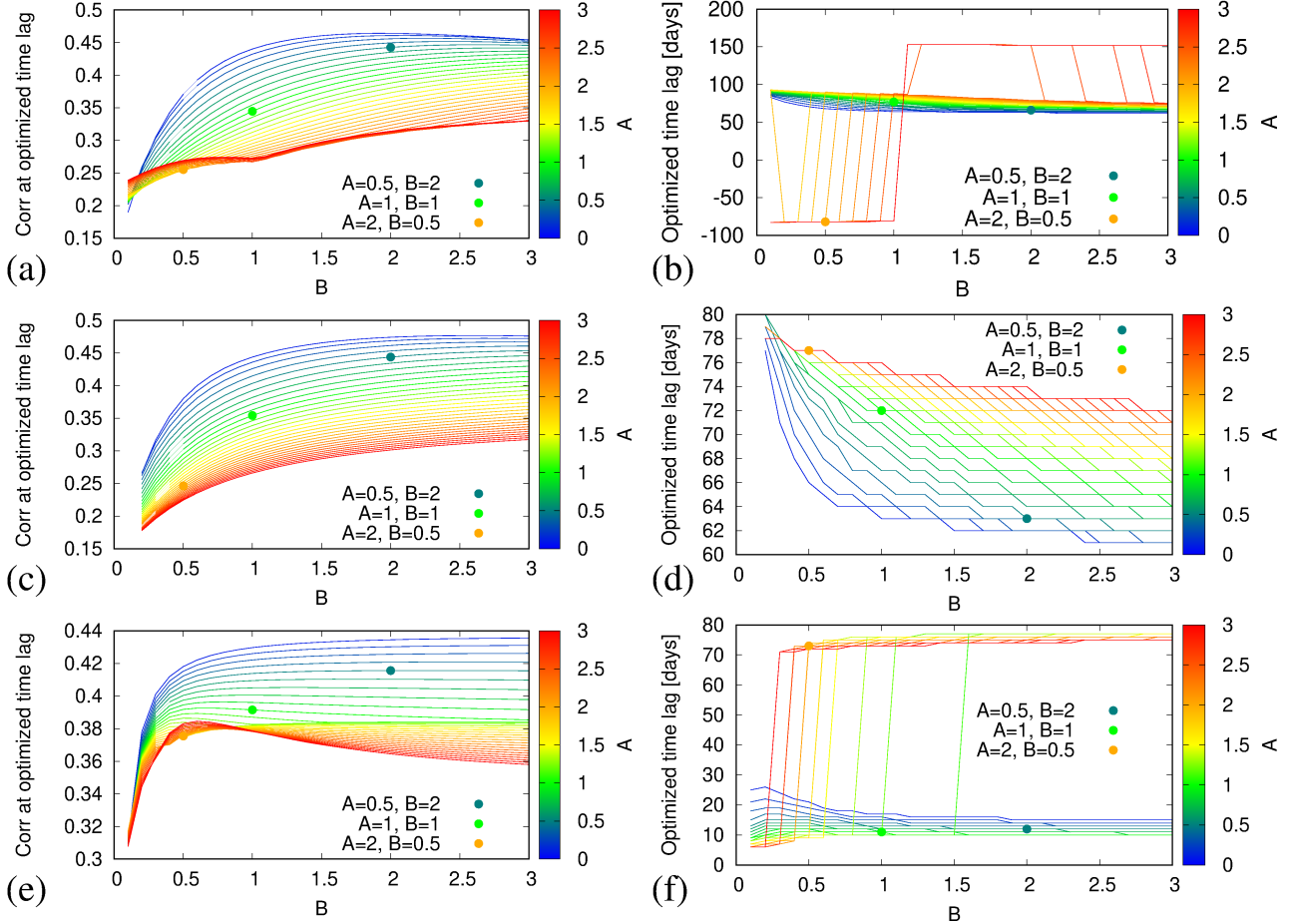


**Figure 7.** Dependence of the maximum correlation and the optimized time-lag on the weights  $A$  and  $B$  in Equation (7). Left column: Maximum correlation over  $B$  for different  $A$  (color coding), using the function  $s^2(t)$  (a), its time-average over 61 days (c) or 201 days (e). Right column: Optimal time-lag, using the function  $s^2(t)$  (b), its time-average over 61 days (d) or 201 days (f). The three particular combinations of  $A$  and  $B$ , as indicated by the colored full circles, will be analyzed in more detail in the next figures.

The left column of Figure 7 shows the maximum correlation (taken at the optimized time-lag shown in the right column) of the modified  $s^2(t)$  function with the 109 merged GLE and S-flare events, when  $A$  and  $B$  are varied. Panels (a), (c), (e) show this for  $s^2(t)$  and its averages over 61

and 201 days, respectively. Panels (b), (d) and (f) on the right show the corresponding optimal time lags. Remarkably, the correlation of 0.35 that was obtained previously for the  $A = B = 1$  case (green full circle in panel (a)) increases to 0.45 when we choose  $A = 0.5$  and  $B = 2$  (blue full circle). This is nearly identical to the maximum correlation obtained with the optimized cosine function, leading hence to very similar low p-values. The other combination,  $A = 2$  and  $B = 0.5$ , gives a reduced correlation of only 0.25, though. These tendencies of the maximum correlation for varying  $A$  and  $B$  are quite robust when choosing longer average times (panels (c) and (e)).

The jumps of the optimal time lags, as seen in panels (b) and (f), are not surprising in view of the similar behaviour that was already visible in Figure 4(d). More surprising is the relatively stable *positive* time-lag of about 70 days as seen in Figure 7(d). Why do solar events usually occur about 70 days *before* the maximum of the tidal forcing? One possible explanation may be related to the finite width of the dominant peaks, which is approximately 90 days according to Figures 5 and 6. Consider the possibility that the waves are predominantly excited not at the maximum of the  $s^2(t)$  function, but in the time intervals of its steepest ascent or descent. Then, positive time lags of 50 days seem not out of reach.

Figure 8 illustrates the relationship between solar events and tidal forcing over the period from 7,000 to 11,000 days after 31 December 1955. Panels (a), (b), and (c) show this for  $s^2(t)$  and its averages over 61 and 201 days, respectively. Each panel comprises curves representing the three combinations of  $A$  and  $B$  that were indicated by the full circles (with the same color) in Figure 7. While the majority of solar events are concentrated around the maxima of  $s^2(t)$ , a few do not fit this pattern. Interestingly, one might get the impression that they are connected to certain side peaks of  $s^2(t)$ , which emerge when using  $A = 2$  and  $B = 0.5$ . The gold question marks in panel (b) indicate this possible link.

A similar link might have been in effect during the last two years. Figure 9 is a modification of Figure 5, showing again the last four GLE events of 2024 and 2025 and the strong X-class flare of 2026 February 1, together with the optimized 629.29-day periodic function. This time, however, we show three  $s^2(t)$  functions for various combinations of  $A$  and  $B$ . While the relationship between the

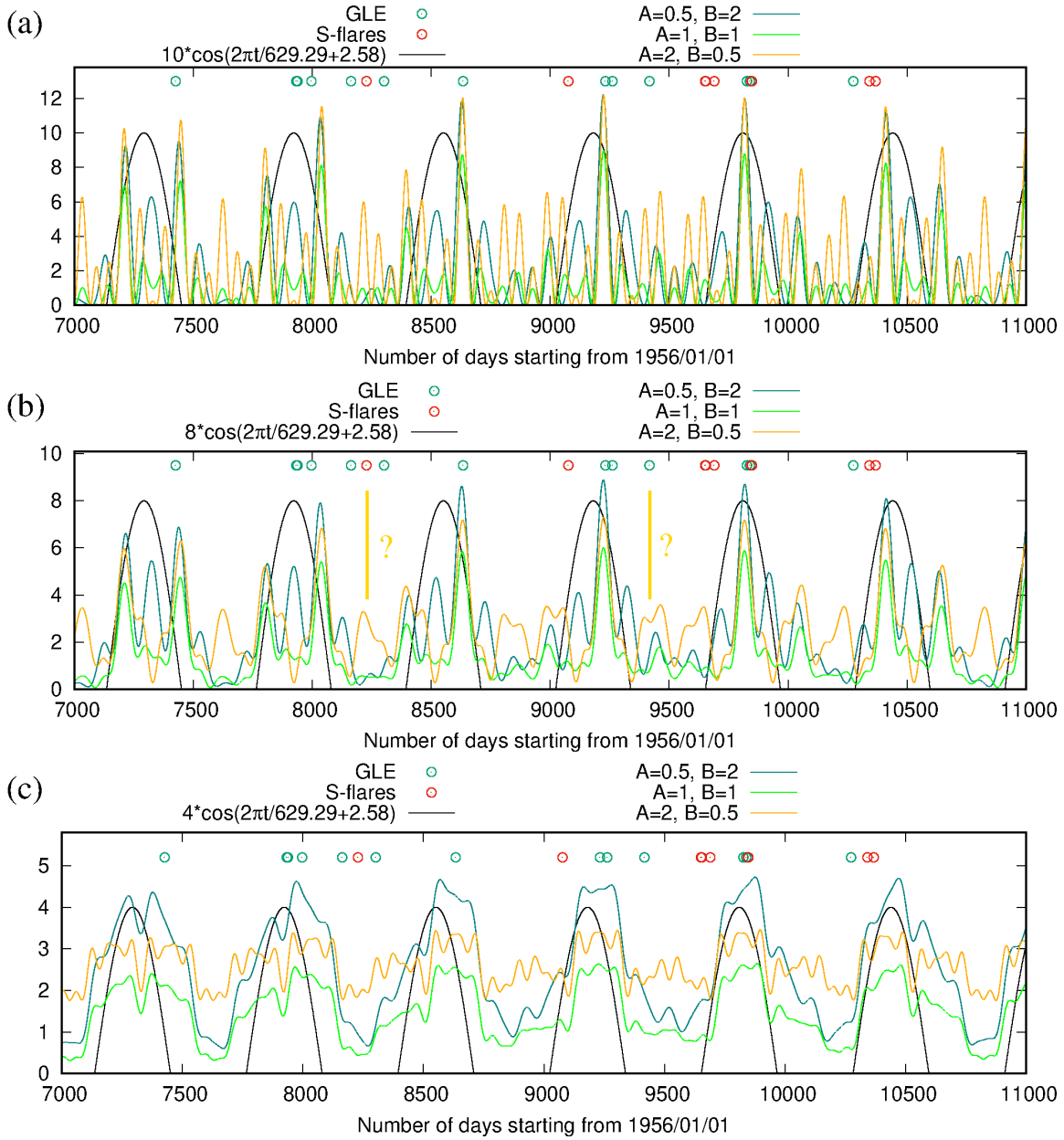


**Figure 8.** (a) GLE and S-flare events, the 629.29-day periodic function optimized for the merger of GLE events and S-flares, and  $s^2(t)$  for three different combinations of  $A$  and  $B$ . (b) The same as (a), but with a time average of the  $s^2(t)$  functions over 61 days. (c) The same as (b), but with a time average over 201 days. The gold question marks in (b) point to a possible link of solar events with side peaks of  $s^2(t)$  for the parameter combination  $A = 2, B = 0.5$ .

main peaks of the three  $s^2(t)$  functions and the 2026 February 1 X-flare, as well as the first two and the last GLE events, remains unchanged, a side peak appears close to the third GLE event for  $A = 2$

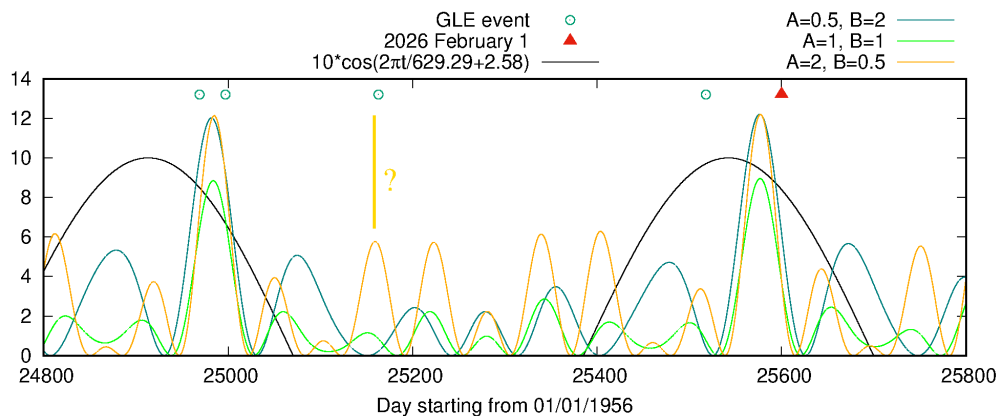


**Figure 9.** The last four GLE events of 2024 and 2025, together with the strong X-class flare of 2026 February 1, the 629.29-day cosine function optimized for the merger of GLE events and S-flares, and  $s^2(t)$  for three different combinations of  $A$  and  $B$ . The gold question mark indicates the possible link of the third GLE event to one of the side peaks of  $s^2(t)$  for the parameter combination  $A = 2$  and  $B = 0.5$ .

and  $B = 0.5$ . The gold question marks in panel (b) indicate a possible link between the side peaks of  $s^2(t)$  and solar events.

In future work we will take into account the dependence of  $A$  and  $B$  on the instantaneous toroidal field. In the most optimistic case, such a detailed investigation may also resolve the apparent contradiction that the case  $A < B$  leads to higher correlation, while the case  $A > B$  may explain the occurrence of some solar events between the main peaks.

#### ACKNOWLEDGMENTS

This work received funding from the Helmholtz Association in frame of the AI project GEOMAGFOR (ZT-I-PF-5-200), and from Deutsche Forschungsgemeinschaft (DFG) in frame of grant No. MA10950/1-1. F.S. thanks Willie Soon for providing an early version of Velasco Herrera et al. (2026), which shows evidence of a 1.7-year signal in S-flare data. He would also like to thank Tony Phillips for inquiring into potential impacts of the January 2026 alignment on solar activity.

#### REFERENCES

- Abreu, J. A., Beer, J., Ferriz-Mas, A., McCracken, K. G., & Steinhilber, F. 2012, *A&A*, 548, 9, doi: [10.1051/0004-6361/201219997](https://doi.org/10.1051/0004-6361/201219997)
- Dikpati, M. 2012, *ApJ*, 745, 128, doi: [10.1088/0004-637X/745/2/128](https://doi.org/10.1088/0004-637X/745/2/128)

- Dikpati, M., & McIntosh, S. W. 2020, *Space Weather*, 18, e2018SW002109, doi: [10.1029/2018SW002109](https://doi.org/10.1029/2018SW002109)
- Dikpati, M., McIntosh, S. W., Bothun, G., et al. 2018, *ApJ*, 853, 144, doi: [10.3847/1538-4357/aaa70d](https://doi.org/10.3847/1538-4357/aaa70d)
- Dröge, W., Gibbs, K., J.M., G., et al. 1990, *Astrophys. J. Suppl. Ser.*, 73, 279, doi: [10.1086/191463](https://doi.org/10.1086/191463)
- Gailitis, A., Gerbeth, G., Gundrum, T., et al. 2018, *J. Plasma Phys.*, 84, 735840301, doi: [10.1017/S0022377818000363](https://doi.org/10.1017/S0022377818000363)
- Horstmann, G. M., Mamatsashvili, G., Giesecke, A., Zaqarashvili, T. V., & Stefani, F. 2023, *ApJ*, 944, doi: [10.3847/1538-4357/aca278](https://doi.org/10.3847/1538-4357/aca278)
- Klevs, M., Stefani, F., & Jouve, L. 2023, *SoPh*, 298, doi: [10.1007/s11207-023-02173-y](https://doi.org/10.1007/s11207-023-02173-y)
- Márquez-Artavia, X., Jones, C. A., & Tobias, S. M. 2017, *Geophys. Astrophys. Fluid Dyn.*, 111, 282, doi: [10.1080/03091929.2017.1301937](https://doi.org/10.1080/03091929.2017.1301937)
- Okhlopkov, V. P. 2016, *Moscow Univ. Phys. Bull.*, 71, 440, doi: [10.3103/S0027134916040159](https://doi.org/10.3103/S0027134916040159)
- Pierron, T., & Forget, F. 2026, *Icarus*, 450, 116984, doi: <https://doi.org/10.1016/j.icarus.2026.116984>
- Raphaldini, B., & Raupp, C. F. M. 2015, *ApJ*, 799, 78, doi: [10.1088/0004-637X/799/1/78](https://doi.org/10.1088/0004-637X/799/1/78)
- Rossby, C.-G. 1939, *J. Mar. Res.*, 2, 38
- Scafetta, N. 2012, *J. Atmos. Sol.-Ter. Phys.*, 81-82, 27, doi: [10.1016/j.jastp.2012.04.002](https://doi.org/10.1016/j.jastp.2012.04.002)
- Scafetta, N., & Bianchini, A. 2022, *Front. Astron. Space Sci*, 9, 937930, doi: [10.3389/fspas.2022.937930](https://doi.org/10.3389/fspas.2022.937930)
- Shirley, J. H. 2023, arXiv:2503.22337, doi: [10.48550/arXiv.2503.22337](https://doi.org/10.48550/arXiv.2503.22337)
- Stefani, F., Giesecke, A., Weber, N., & Weier, T. 2016, *SoPh*, 291, 2197, doi: [10.1007/s11207-016-0968-0](https://doi.org/10.1007/s11207-016-0968-0)
- Stefani, F., Giesecke, A., & Weier, T. 2019, *SoPh*, 294, 60, doi: [10.1007/s11207-019-1447-1](https://doi.org/10.1007/s11207-019-1447-1)
- Stefani, F., Horstmann, G. M., Klevs, M., Mamatsashvili, G., & Weier, T. 2024, *SoPh*, 299, doi: [10.1007/s11207-024-02295-x](https://doi.org/10.1007/s11207-024-02295-x)
- Stefani, F., Horstmann, G. M., Mamatsashvili, G., & Weier, T. 2025, *SoPh*, 300, doi: [10.1007/s11207-025-02521-0](https://doi.org/10.1007/s11207-025-02521-0)
- Stefani, F., Stepanov, R., & Weier, T. 2021, *SoPh*, 296, 88, doi: [10.1007/s11207-021-01822-4](https://doi.org/10.1007/s11207-021-01822-4)
- Tan, B., Zhang, Y., Huang, J., & Ji, K. 2025, *ApJL*, 979, doi: [10.3847/2041-8213/ada611](https://doi.org/10.3847/2041-8213/ada611)
- Velasco Herrera, V. M., Perez-Peraza, J., Soon, W., & Marquez-Adame, J. C. 2018, *New Astron.*, 60, 7, doi: [10.1016/j.newast.2017.09.007](https://doi.org/10.1016/j.newast.2017.09.007)
- Velasco Herrera, V. M., Velasco Herrera, G., Soon, W., et al. 2026, *J. Geophys. Res. Space Phys.*, 131, doi: [10.1029/2025JA034977](https://doi.org/10.1029/2025JA034977)
- Weber, M. A., Fan, Y., & Miesch, M. S. 2011, *ApJ*, 741, doi: [10.1088/0004-637X/741/1/11](https://doi.org/10.1088/0004-637X/741/1/11)
- Weber, N., Galindo, V., Stefani, F., & Weier, T. 2015, *New J. Phys.*, 17, 113013, doi: [10.1088/1367-2630/17/11/113013](https://doi.org/10.1088/1367-2630/17/11/113013)

Wilson, I. R. G. 2013, *Pattern Recogn. Phys.*, 1, 147, doi: [10.5194/prp-1-147-2013](https://doi.org/10.5194/prp-1-147-2013)

Zaqarashvili, T. V., Carbonell, M., Oliver, R., & Ballester, J. L. 2010a, *ApJ*, 709, 749, doi: [10.1088/0004-637X/709/2/749](https://doi.org/10.1088/0004-637X/709/2/749)

—. 2010b, *ApJL*, 724, L95,

doi: [10.1088/2041-8205/724/1/L95](https://doi.org/10.1088/2041-8205/724/1/L95)

Zaqarashvili, T. V., Albeikioni, M., Ballester, J. L., et al. 2021, *Space Sci. Rev.*, 217, 15,

doi: [10.1007/s11214-021-00790-2](https://doi.org/10.1007/s11214-021-00790-2)